

MHD flow of non-Newtonian ferro nanofluid between two vertical porous walls with Cattaneo–Christov heat flux, entropy generation, and time-dependent pressure gradient

Anala Subramanyam Reddy^a , Somasundaram Rajamani^{a,b,1} ,
Ali J. Chamkha^c , Suripeddi Srinivas^d , Krishnamurthy Jagadeshkumar^a 

^aDepartment of Mathematics, School of Advanced Sciences,
Vellore Institute of Technology,
Vellore-632014, India

^bDepartment of Mathematics,
Einstein College of Arts and Science,
Seetharpanallur, Tirunelveli-627012, India
sraja199317@gmail.com

^cFaculty of Engineering,
Kuwait College of Science and Technology,
Doha District-35004, Kuwait

^dDepartment of Mathematics, School of Advanced Sciences,
VIT-AP University, Inavolu,
Amaravati-522237, India

Received: July 15, 2022 / **Revised:** February 22, 2023 / **Published online:** April 27, 2023

Abstract. This article studies the magnetohydrodynamic flow of non-Newtonian ferro nanofluid subject to time-dependent pressure gradient between two vertical permeable walls with Cattaneo–Christov heat flux and entropy generation. In this study, blood is considered as non-Newtonian fluid (couple stress fluid). Nanoparticles' shape factor, Joule heating, viscous dissipation, and radiative heat impacts are examined. This investigation is crucial in nanodrug delivery, pharmaceutical processes, microelectronics, biomedicines, and dynamics of physiological fluids. The flow governing partial differential equations are transformed into the system of ordinary differential equations by deploying the perturbation process and then handled with Runge–Kutta 4th-order procedure aided by the shooting approach. Hamilton–Crosser model is employed to analyze the thermal conductivity of different shapes of nanoparticles. The obtained results reveal that intensifying Eckert number leads to a higher temperature, while the reverse is true for increased thermal relaxation parameter. Heat transfer rate escalates for increasing thermal radiation. Entropy dwindles for intensifying thermal relaxation parameter.

Keywords: entropy generation, Cattaneo–Christov heat flux, couple stress ferro nanofluid, MHD, pressure gradient, thermal radiation.

¹Corresponding author.

1 Introduction

In engineering, science, and industries, non-Newtonian fluids taking the body couple stress into consideration are widely used, and they are relevant particularly in common engineering fluids where tiny ingredients are crucial like polymer extrusion, dissolvent, crystallization of liquids, lubricants, biofluids, and synovial fluids [7, 24, 25]. To account for the mechanical interactions between fluid particles, Stokes [26] developed a couple stress theory that relied on a continuum concept. The author analysed the kinetic characteristics of electrically conductive couple stress fluid on hydromagnetic field. By adopting the modified Adomian decomposition method, Adesanya and Makinde [1] examined the significance of couple stresses on incompressible viscous fluids flowing through permeable channel with regard to entropy analysis. A blood flow analysis with the inspection of rhythmic flow in non-Newtonian hybrid nanofluid considered body couples between parallel permeable walls in the presence of radiative heat flux, Ohmic and viscous dissipations by employing Runge–Kutta 4th-order procedure aided by the shooting approach is done by Rajamani and Reddy [19]. Nowadays many investigators and researchers are greatly acknowledged the field of thermal and mass transport due to its episodes in laser treatments, heat exchangers, and food processing. Fourier [9] concept of heat diffusion signifies that the temperature equation is parabolic, and it is imprecise due to the temperature gradient with shortcomings (zero-time lag). Cattaneo [3] modified the Fourier's heat conduction model with thermal relaxation time, which permits the thermal distribution from the beginning to end with the constrained rapidity. But the thermal relaxation factor differs for materials invariance. To address this inconvenience, Christov [6] developed the Oldroyd's upper convected derivatives for the Cattaneo's heat flux model with the terminology of Cattaneo–Christov heat flux model. Waqas et al. [30] examined the entropy analysis and Cattaneo–Christov theory on nanofluid flow in a rocket engine nozzle under the influence of radiative heat flux.

Nanofluids play an important role as a heat transfer medium in biomedical applications (nanodrug delivery, imaging and sensing, cryopreservation, nano-cryosurgery, cancer therapies), lubrication, electronics, desalination, detergency, machining, building heating, heat exchangers, and radiators [12, 16, 20]. Choi [5] pioneered the concept of nanofluids by adding the nano-size (1–100 nm) particles into the base fluid (conventional fluid) and witnessed the outstanding performance of heat transfer fluid. Hamilton and Crosser [14] investigated the effect of particle shape, structure, and interparticle interaction on the thermodynamic properties of a heterogeneous mixture with continuous and discontinuous forms. Sheikholeslemi et al. [23] examined the heat transfer flow of ferro nanofluid in a pair of moving permeable walls by employing the control volume based finite element method in the presence of shape factor effect. Hosseinzadeh et al. [15] focused on the flow of ferro nanofluid with various base fluids by adopting Runge–Kutta 5th-order scheme in the presence of magnetic field with shape factor analysis. Timofeeva et al. [27] investigated the viscosity and thermal conductivity of different nanoparticles' shapes of alumina-ethylene glycol+water nanofluid by employing Hamilton–Crosser model with experimental data accompanied by theoretical modelling. Entropy is often thought of to measure the power that is ineffective for productive work. Entropy analysis

is useful in solar energy, coolers, nuclear reactors, and air chillers. Kumawat et al. [17] studied the entropy analysis on hydromagnetic blood flow in a stenosed artery by adopting finite difference scheme. Sharma et al. [21] investigated the entropy generation of blood based fusion of gold-alumina nanofluid in a tapered multi-stenosed artery with radiative heat flux and magnetic field by employing Crank–Nicolson scheme. Basha and Sivraj [2] adopted the weighted residual scheme for the application of blood flow in wounded tissues by studying the heat transmission and entropy analysis of ferro-blood nanofluid in a circular permeable tube.

Pulsatile flow is characterized by the combination of steady and rhythmic time fluctuating components. With only oscillation (i.e., steady flow component is zero), the pulsating flow becomes oscillating flow. Studying pressure-induced pulsatile flow is crucial because it occurs in bioindustrial equipment, pulse jet engines, dynamics of bio and synovial fluids, coastal environments [4, 8, 13, 18, 28, 31]. Shawky [22] made an attempt to analyse the pulsatile flow of Ree–Eyring fluid via channel by employing Lightill approach in the presence of Ohmic and viscous dissipations. Gad [10] inspected the pulsating flow of magneto nanofluid between the pair of parallel walls with the aid of perturbation approach with Hall effect. Wang et al. [29] examined the pulsating hydromagnetic non-Newtonian fluid flow in a small vessel by using finite difference algorithm with Ohmic and viscous dissipations. Under the influence of radiative heat flux and Joule heating, Govindarajulu and Reddy [11] utilized Runge–Kutta 4th-order procedure aided by the shooting approach to model the rhythmic hydromagnetic flow of 3rd-grade hybrid nanofluid between parallel permeable walls.

The aforementioned studies reveal that there is no study so far related to magneto-hydrodynamic (MHD) non-Newtonian ferro nanofluid flow subject to time-dependent pressure gradient between two vertical permeable walls with Cattaneo–Christov heat flux and entropy generation. In this analysis, the blood and Fe_3O_4 are preferred as the non-Newtonian (couple stress fluid) conventional fluid and nanoparticles, respectively. The purpose of this work is to explore the simultaneous influence of radiative heat flux, Ohmic and viscous dissipations on pulsatile hydromagnetic couple stress ferro nanofluid between a vertical permeable parallel walls subject to Cattaneo–Christov theory with the analysis of shape factor and entropy generation. By deploying the perturbation approach, the flow model equations (partial differential equations) are reduced to set of ordinary differential equations and handled with Runge–Kutta 4th-order procedure aided by the shooting technique. The present work is significant in the field of nanodrug delivery, pharmaceutical processes, dynamics of physiological fluids, and biomedicines. The profiles of temperature, entropy generation, Bejan number, and phase lag analysis for various values of pertinent parameters are drawn graphically and discussed in detail. Heat transfer rate of couple stress ferro nanofluid for various emerging parameters is tabulated and explained in detail.

2 Formulation of the problem

In this study, an incompressible, laminar, electrically conducting MHD flow of couple stress ferro nanofluid induced by time-dependent pressure gradient in a vertical porous

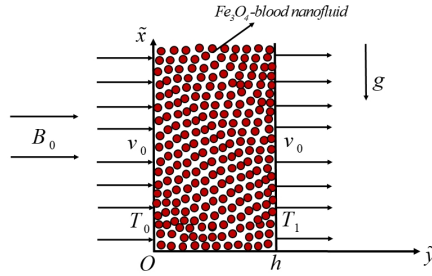


Figure 1. Coordinate system of the current flow.

channel is deliberated. Blood is picked up as couple stress fluid (non-Newtonian base fluid), and Fe_3O_4 is picked as nanoparticle. Radiative heat flux, Ohmic and viscous dissipations are considered. The physical sketch of the current study is presented in Fig. 1. Flow is induced by applying a magnetic field of equal intensity B_0 normal to the nanofluid flow. T_1 and T_0 are the wall temperatures at right and left walls, correspondingly ($T_0 < T_1$). The Cattaneo–Christov heat flux model is incorporated with the energy equation. With the same velocity v_0 , the fluid is driven past the left wall and drawn from the right wall. Under these hypotheses, the governing equations of the current model are [6, 25, 26]

$$\frac{\partial \tilde{u}}{\partial \tilde{t}} + v_0 \frac{\partial \tilde{u}}{\partial \tilde{y}} = -\frac{1}{\rho_{nf}} \frac{\partial \tilde{P}}{\partial \tilde{x}} + \frac{\mu_{nf}}{\rho_{nf}} \frac{\partial^2 \tilde{u}}{\partial \tilde{y}^2} - \frac{\eta}{\rho_{nf}} \frac{\partial^4 \tilde{u}}{\partial \tilde{y}^4} - \frac{\sigma_{nf} B_0^2}{\rho_{nf}} \tilde{u} + \frac{g(\rho\beta)_{nf}}{\rho_{nf}} (\tilde{T} - T_0), \tag{1}$$

$$\begin{aligned} \frac{\partial \tilde{T}}{\partial \tilde{t}} + v_0 \frac{\partial \tilde{T}}{\partial \tilde{y}} + \lambda_2 \left[\frac{\partial^2 \tilde{T}}{\partial \tilde{t}^2} + 2v_0 \frac{\partial^2 \tilde{T}}{\partial \tilde{t} \partial \tilde{y}} + v_0^2 \frac{\partial^2 \tilde{T}}{\partial \tilde{y}^2} \right] \\ = \frac{k_{nf}}{(\rho C_p)_{nf}} \frac{\partial^2 \tilde{T}}{\partial \tilde{y}^2} + \frac{\mu_{nf}}{(\rho C_p)_{nf}} \left(\frac{\partial \tilde{u}}{\partial \tilde{y}} \right)^2 + \frac{\eta}{(\rho C_p)_{nf}} \left(\frac{\partial^2 \tilde{u}}{\partial \tilde{y}^2} \right)^2 - \frac{1}{(\rho C_p)_{nf}} \frac{\partial \tilde{q}_r}{\partial \tilde{y}} \\ + \frac{\sigma_{nf} B_0^2}{(\rho C_p)_{nf}} \tilde{u}^2, \end{aligned} \tag{2}$$

where \tilde{u} is the velocity component of \tilde{x} direction, μ_{nf} , ρ_{nf} , $(\rho C_p)_{nf}$, σ_{nf} , k_{nf} represent the viscosity, density, heat capacitance, electrical conductivity, and thermal conductivity of the nanofluid, and the subscripts nf , f , and s denote nanofluid, base fluid (blood), and Fe_3O_4 nanoparticles, respectively. \tilde{T} is the temperature of nanofluid, η is coefficient of couple stress viscosity, λ_2 is the relaxation time for heat flux, and the radiative heat flux is denoted as \tilde{q}_r . The pertinent boundary conditions (B.Cs) are given by [1, 7, 26]:

$$\begin{aligned} \tilde{u} = 0, \quad \frac{\partial^2 \tilde{u}}{\partial \tilde{y}^2} = 0, \quad \tilde{T} = T_0 \quad \text{at } \tilde{y} = 0, \\ \tilde{u} = 0, \quad \frac{\partial^2 \tilde{u}}{\partial \tilde{y}^2} = 0, \quad \tilde{T} = T_1 \quad \text{at } \tilde{y} = h. \end{aligned}$$

Table 1. The thermophysical characteristics of Fe₃O₄ nanoparticles and blood [2, 15].

Property	Fe ₃ O ₄	Blood
ρ [kg/m ³]	5200	1050
k [W/(mK)]	6	0.52
C_p [J/(kgK)]	670	3617
σ [1/(Ω m)]	25000	0.8
β [1/K]	1.3×10^{-5}	1.8×10^{-6}

Table 2. Sphericity, shape factor and viscosity intensification coefficients β_1 and β_2 for various shapes of nanoparticles [15, 27].

Nanoparticles' shapes	Aspect ratio	Sphericity ξ	Shape factor $n = 3/\xi$	β_1	β_2
Bricks	1 : 1 : 1	0.81	3.7	1.9	471.9
Cylinders	1 : 8	0.62	4.9	13.5	904.4
Blades	1 : 6 : 1/12	0.36	8.6	14.6	123.3
Platelets	1 : 1/8	0.52	5.7	31.6	612.6

The thermal and physical characteristics of blood (conventional fluid) and Fe₃O₄ nanoparticles are prearranged in Table 1, and shape factor details of various shapes of nanoparticles are listed in Table 2 and are given as [2, 15, 21]

$$\rho_{nf} = (1 - \phi)\rho_f + \phi\rho_s, \quad (\rho C_p)_{nf} = (1 - \phi)(\rho C_p)_f + \phi(\rho C_p)_s,$$

$$(\rho\beta)_{nf} = (1 - \phi)(\rho\beta)_f + \phi(\rho\beta)_s, \quad \frac{\sigma_{nf}}{\sigma_f} = 1 + \frac{3\left(\frac{\sigma_s}{\sigma_f} - 1\right)\phi}{\left(\frac{\sigma_s}{\sigma_f} + 2\right) - \left(\frac{\sigma_s}{\sigma_f} - 1\right)\phi}.$$

The dynamical viscosity of nanofluid is given by [14, 27]:

$$\mu_{nf} = \begin{cases} \frac{\mu_f}{(1-\phi)^{2.5}} & \text{(spherical case),} \\ \mu_f(1 + \beta_1\phi + \beta_2\phi^2) & \text{(nonspherical case).} \end{cases} \tag{3}$$

Thermal conductivity of nanofluid is calculated by Hamilton–Crosser model [14, 27] and is given by

$$\frac{k_{nf}}{k_f} = \frac{k_s + (n - 1)k_f - (n - 1)\phi(k_f - k_s)}{k_s + (n - 1)k_f + \phi(k_f - k_s)}. \tag{4}$$

By adopting the Rosseland estimation for thermal radiative flux (\tilde{q}_r) and following [21, 30], Eq. (2) becomes

$$\begin{aligned} & \frac{\partial \tilde{T}}{\partial \tilde{t}} + v_0 \frac{\partial \tilde{T}}{\partial \tilde{y}} + \lambda_2 \left[\frac{\partial^2 \tilde{T}}{\partial \tilde{t}^2} + 2v_0 \frac{\partial^2 \tilde{T}}{\partial \tilde{t} \partial \tilde{y}} + v_0^2 \frac{\partial^2 \tilde{T}}{\partial \tilde{y}^2} \right] \\ & = \frac{k_{nf}}{(\rho C_p)_{nf}} \frac{\partial^2 \tilde{T}}{\partial \tilde{y}^2} + \frac{\mu_{nf}}{(\rho C_p)_{nf}} \left(\frac{\partial \tilde{u}}{\partial \tilde{y}} \right)^2 + \frac{\eta}{(\rho C_p)_{nf}} \left(\frac{\partial^2 \tilde{u}}{\partial \tilde{y}^2} \right)^2 \\ & \quad + \frac{1}{(\rho C_p)_{nf}} \frac{16}{3} \frac{\tilde{\sigma} T_1^3}{\aleph} \frac{\partial^2 \tilde{T}}{\partial \tilde{y}^2} + \frac{\sigma_{nf} B_0^2}{(\rho C_p)_{nf}} \tilde{u}^2, \end{aligned} \tag{5}$$

where \aleph is mean absorption coefficient, and $\tilde{\sigma}$ is Stefan–Boltzmann constant.

Now, with the aid of below dimensionless parameters and variables,

$$\begin{aligned} \tilde{x} &= xh, & \tilde{y} &= yh, & \tilde{t} &= \frac{t}{\omega}, & \tilde{u} &= Uu, & \tilde{P} &= \frac{P\mu_f U}{h}, \\ \tilde{T} &= T_0 + \theta(T_1 - T_0), & H &= \frac{\sqrt{\omega}h}{\sqrt{\nu_f}}, & M &= B_0h\sqrt{\frac{\sigma_f}{\mu_f}}, & \delta &= \lambda_2\omega, \\ Pr &= \frac{\nu_f(\rho C_P)_f}{k_f}, & Ec &= \frac{U^2}{(C_P)_f(T_1 - T_0)}, & R &= \frac{v_0h}{\nu_f}, \\ Re &= \frac{Uh}{\nu_f}, & Rd &= \frac{4\tilde{\sigma}T_1^3}{\aleph k_f}, & \lambda &= \frac{\eta}{\mu_f h^2}, & Gr &= \frac{g\beta_f(T_1 - T_0)h^3}{\nu_f^2}. \end{aligned}$$

Equations (1) and (5) become

$$\begin{aligned} \frac{\partial u}{\partial t} + \frac{R}{H^2} \frac{\partial u}{\partial y} \\ = -\frac{1}{A_1 H^2} \frac{\partial P}{\partial x} + \frac{A_2}{A_1 H^2} \frac{\partial^2 u}{\partial y^2} - \frac{\lambda}{A_1 H^2} \frac{\partial^4 u}{\partial y^4} - \frac{A_5 M^2}{A_1 H^2} u + \frac{A_6 Gr}{A_1 H^2 Re} \theta, \end{aligned} \quad (6)$$

$$\begin{aligned} \frac{\partial \theta}{\partial t} + \frac{R}{H^2} \frac{\partial \theta}{\partial y} + \delta \left[\frac{\partial^2 \theta}{\partial t^2} + \frac{2R}{H^2} \frac{\partial^2 \theta}{\partial t \partial y} + \frac{R^2}{H^4} \frac{\partial^2 \theta}{\partial y^2} \right] \\ = \frac{(A_4 + \frac{4}{3}Rd)}{A_3 Pr H^2} \frac{\partial^2 \theta}{\partial y^2} + \frac{A_2 Ec}{A_3 H^2} \left(\frac{\partial u}{\partial y} \right)^2 + \frac{\lambda Ec}{A_3 H^2} \left(\frac{\partial^2 u}{\partial y^2} \right)^2 + \frac{A_5 Ec M^2}{A_3 H^2} u^2. \end{aligned} \quad (7)$$

Here

$$\begin{aligned} A_1 &= (1 - \phi) + \phi \frac{\rho_s}{\rho_f}, & A_2 &= \frac{1}{(1 - \phi)^{2.5}}, \\ A_3 &= (1 - \phi) + \phi \frac{(\rho C_P)_s}{(\rho C_P)_f}, & A_4 &= \frac{k_s + (n - 1)k_f - (n - 1)\phi(k_f - k_s)}{k_s + (n - 1)k_f + \phi(k_f - k_s)}, \\ A_5 &= 1 + \frac{3(\frac{\sigma_s}{\sigma_f} - 1)\phi}{(\frac{\sigma_s}{\sigma_f} + 2) - (\frac{\sigma_s}{\sigma_f} - 1)\phi}, & A_6 &= (1 - \phi) + \phi \frac{(\rho\beta)_s}{(\rho\beta)_f}, \end{aligned}$$

Ec is the Eckert number, R is cross flow Reynolds number, M is Hartmann number, Pr is the Prandtl number, H is frequency parameter, Gr is the Grashof number, Re is the Reynolds number, Rd is radiation parameter, λ is couple stress parameter, δ is thermal relaxation parameter, ϕ is the volume fraction of nanoparticles.

The B.Cs are as follows:

$$\begin{aligned} u = 0, & \quad \frac{\partial^2 u}{\partial y^2} = 0, & \theta = 0 & \quad \text{at } y = 0, \\ u = 0, & \quad \frac{\partial^2 u}{\partial y^2} = 0, & \theta = 1 & \quad \text{at } y = 1. \end{aligned}$$

2.1 Analysis of entropy generation

The entropy generation of the present work in dimensional form is given as [1, 21, 30]

$$N_s = \frac{k_{nf}}{T_0^2} \left(1 + \frac{16}{3} \frac{\tilde{\sigma} T_1^3}{\aleph k_f} \right) \left(\frac{\partial \tilde{T}}{\partial \tilde{y}} \right)^2 + \frac{\mu_{nf}}{T_0} \left(\frac{\partial \tilde{u}}{\partial \tilde{y}} \right)^2 + \frac{\eta}{T_0} \left(\frac{\partial^2 \tilde{u}}{\partial \tilde{y}^2} \right)^2 + \frac{\sigma_{nf} B_0^2}{T_0} \tilde{u}^2,$$

$$N_s = N_t + N_v + N_j.$$

Here

$$N_t = \frac{k_{nf}}{T_0^2} \left(1 + \frac{16}{3} \frac{\tilde{\sigma} T_1^3}{\aleph k_f} \right) \left(\frac{\partial \tilde{T}}{\partial \tilde{y}} \right)^2, \quad N_v = \frac{\mu_{nf}}{T_0} \left(\frac{\partial \tilde{u}}{\partial \tilde{y}} \right)^2 + \frac{\eta}{T_0} \left(\frac{\partial^2 \tilde{u}}{\partial \tilde{y}^2} \right)^2,$$

$$N_j = \frac{\sigma_{nf} B_0^2}{T_0} \tilde{u}^2$$

represent thermal irreversibility, fluid friction (viscous and couple stress) irreversibility, and Joule heating irreversibility, respectively.

The nondimensional form of entropy is

$$NG = A_4 \left(1 + \frac{4}{3} Rd \right) \left(\frac{\partial \theta}{\partial y} \right)^2 + \frac{A_2 Ec Pr}{\Omega} \left(\frac{\partial u}{\partial y} \right)^2 + \frac{\lambda Ec Pr}{\Omega} \left(\frac{\partial^2 u}{\partial y^2} \right)^2 + \frac{A_5 M^2 Ec Pr}{\Omega} u^2. \tag{8}$$

Here $NG = T_0 h^2 N_s / ((T_1 - T_0)^2 k_f)$ is the characteristic entropy production rate, $\Omega = (T_1 - T_0) / T_0$ is the temperature variance measuring parameter. The Bejan number (Be) is elucidated as the ratio between the thermal irreversibility and the total entropy generation, and it is expressed as

$$Be = \frac{A_4 \left(1 + \frac{4}{3} Rd \right) \left(\frac{\partial \theta}{\partial y} \right)^2}{A_4 \left(1 + \frac{4}{3} Rd \right) \left(\frac{\partial \theta}{\partial y} \right)^2 + \frac{A_2 Ec Pr}{\Omega} \left(\frac{\partial u}{\partial y} \right)^2 + \frac{\lambda Ec Pr}{\Omega} \left(\frac{\partial^2 u}{\partial y^2} \right)^2 + \frac{A_5 M^2 Ec Pr}{\Omega} u^2}.$$

3 Solution of the problem

It is presupposed that the current flow is persuaded by the pulsatile pressure gradient, and it is presumed in the following form [16, 18]:

$$-\frac{\partial P}{\partial x} = \lambda_0 + \varepsilon \lambda_1 e^{it}. \tag{9}$$

Here P is the dimensionless fluid pressure, $\varepsilon (\ll 1)$ is a positive quantity, t is dimensionless time, and λ_0, λ_1 are steady and unsteady magnitudes of pulsatile pressure gradient.

On account of Eq. (9), the solution terms for u and θ can be considered as

$$u(y, t) = u_0(y) + \varepsilon u_1(y) \exp(it), \tag{10}$$

$$\theta(y, t) = \theta_0(y) + \varepsilon \theta_1(y) \exp(it). \tag{11}$$

Now, by substituting Eq. (9)–(11) into Eqs. (6), (7) and likening the coefficients of like powers of ε , one can attain

$$A_2 \frac{d^2 u_0}{dy^2} - \lambda \frac{d^4 u_0}{dy^4} - A_1 R \frac{du_0}{dy} - A_5 M^2 u_0 + \frac{A_6 Gr}{Re} \theta_0 + \lambda_0 = 0, \quad (12)$$

$$A_2 \frac{d^2 u_1}{dy^2} - \lambda \frac{d^4 u_1}{dy^4} - A_1 R \frac{du_1}{dy} - A_5 M^2 u_1 - i A_1 H^2 u_1 + \frac{A_6 Gr}{Re} \theta_1 + \lambda_1 = 0, \quad (13)$$

$$\begin{aligned} & \frac{(A_4 + \frac{4}{3} R d)}{Pr} \frac{d^2 \theta_0}{dy^2} - \frac{A_3 \delta R^2}{H^2} \frac{d^2 \theta_0}{dy^2} - A_3 R \frac{d\theta_0}{dy} + A_2 Ec \left(\frac{du_0}{dy} \right)^2 \\ & + \lambda Ec \left(\frac{d^2 u_0}{dy^2} \right)^2 + A_5 M^2 Ec u_0^2 = 0, \end{aligned} \quad (14)$$

$$\begin{aligned} & \frac{(A_4 + \frac{4}{3} R d)}{Pr} \frac{d^2 \theta_1}{dy^2} - \frac{A_3 \delta R^2}{H^2} \frac{d^2 \theta_1}{dy^2} - (2i\delta + 1) A_3 R \frac{d\theta_1}{dy} - (i - \delta) A_3 H^2 \theta_1 \\ & + 2A_2 Ec \frac{du_0}{dy} \frac{du_1}{dy} + 2\lambda Ec \frac{d^2 u_0}{dy^2} \frac{d^2 u_1}{dy^2} + 2A_5 M^2 Ec u_0 u_1 = 0. \end{aligned} \quad (15)$$

The associated B.Cs are

$$\begin{aligned} u_0(0) &= 0, & \frac{d^2 u_0}{dy^2}(0) &= 0, & \theta_0(0) &= 0, \\ u_0(1) &= 0, & \frac{d^2 u_0}{dy^2}(1) &= 0, & \theta_0(1) &= 1, \\ u_1(0) &= 0, & \frac{d^2 u_1}{dy^2}(0) &= 0, & \theta_1(0) &= 0, \\ u_1(1) &= 0, & \frac{d^2 u_1}{dy^2}(1) &= 0, & \theta_1(1) &= 0. \end{aligned} \quad (16)$$

On account of Eq. (9), the expression for NG can be considered as

$$NG(y, t) = NG_0(y) + \varepsilon NG_1(y) e^{st}.$$

Now, by substituting Eqs. (10), (11) into Eq. (8) and likening the coefficients of like powers of ε , one can attain

$$\begin{aligned} NG_0 &= A_4 \left(1 + \frac{4}{3} R d \right) \left(\frac{\partial \theta_0}{\partial y} \right)^2 + \frac{A_2 Ec Pr}{\Omega} \left(\frac{\partial u_0}{\partial y} \right)^2 + \frac{\lambda Ec Pr}{\Omega} \left(\frac{\partial^2 u_0}{\partial y^2} \right)^2 \\ &+ \frac{A_5 M^2 Ec Pr}{\Omega} u_0^2, \\ NG_1 &= 2A_4 \left(1 + \frac{4}{3} R d \right) \left(\frac{\partial \theta_0}{\partial y} \right) \left(\frac{\partial \theta_1}{\partial y} \right) + \frac{2A_2 Ec Pr}{\Omega} \left(\frac{\partial u_0}{\partial y} \right) \left(\frac{\partial u_1}{\partial y} \right) \\ &+ \frac{2\lambda Ec Pr}{\Omega} \left(\frac{\partial^2 u_0}{\partial y^2} \right) \left(\frac{\partial^2 u_1}{\partial y^2} \right) + \frac{2A_5 M^2 Ec Pr}{\Omega} u_0 u_1. \end{aligned}$$

Table 3. Comparative study between the current results and NDSolve for Nu at $y = 0$ for influence of Ec , λ , and Rd when $M = 2$, $R = 1$, $\lambda = 0.2$, $\delta = 0.1$, $H = 3$, $Pr = 21$, $Ec = 0.6$, $Rd = 2$, $Gr = 4$, $Re = 1$, $\varepsilon = 0.001$, and $t = \pi/4$.

Parameter	Values	Present results $(Nu)_{y=0}$	NDSolve $(Nu)_{y=0}$
Ec	0.2	0.118706028	0.118706066
	0.4	0.187939861	0.187941234
	0.6	0.277138365	0.277148189
λ	0.5	0.148679025	0.148679035
	1	0.103431075	0.103438085
	1.5	0.088973029	0.088973356
Rd	1	0.063282946	0.063283620
	1.5	0.135393587	0.135393591
	2	0.277138365	0.277138365

An essential physical parameter, the dimensionless Nusselt number, is delineated at the walls as [16, 18, 30]

$$Nu = \left(A_4 + \frac{4}{3} Rd \right) \left(\frac{\partial \theta}{\partial y} \right)_{y=0,1}.$$

Now, the set of Eqs. (12)–(15) along with the B.Cs (16) are deciphered numerically with the shooting approach aided by Runge–Kutta 4th-order procedure. The step extent is taken as 0.001, precision is static for the convergence criteria.

To ensure the precision of the current outcomes, we done a comparison between the current outcomes and the outcomes attained by NDSolve using MATHEMATICA, which are prearranged in Table 3. It is witnessed that there is a worthy settlement between the present results and the outcomes attained by NDSolve.

4 Result and discussion

The present segment explores the influence of nanoparticle’s shape factor, viscous dissipation, applied magnetic field, Cattaneo–Christov heat flux, Joule heating, and thermal radiation on the flow variables of couple stress ferro nanofluid between permeable parallel walls with the help of graphical results, which are present in Figs. 2–4. In this study, the values of pertinent parameters are considered as $M = 2$, $\lambda = 0.2$, $\delta = 0.1$, $R = 1$, $H = 3$, $Pr = 21$, $Ec = 0.4$, $Rd = 2$, $Gr = 5$, $Re = 1$, $\varepsilon = 0.001$, and $t = \pi/9$.

In this analysis, θ_s , θ_t , Nu_s , Nu_t represent steady temperature, unsteady temperature, steady heat transfer rate, and unsteady heat transfer rate of couple stress ferro nanofluid, respectively. The influence of different shapes of ferro nanoparticles on temperature, heat transfer rate, entropy generation, and Bejan number is depicted in Figs. 2(a)–2(d). Figure 2(a) shows that the spherical shape of ferro nanoparticles has greater influence on temperature of nanofluid compared to other shapes. The spherical shape nanoparticles has performed well on heat transfer phenomena compared with other shapes (see Fig. 2(b)) due to their high binding capacity and dispersibility. The spherical shape has an advantage

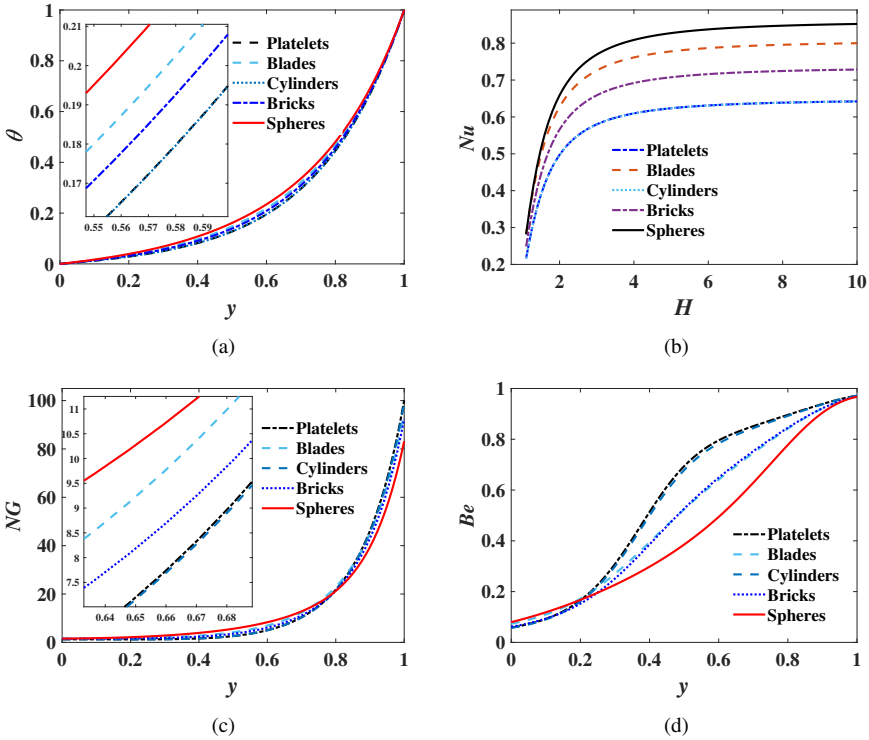


Figure 2. Shape factor effect on (a) temperature, (b) heat transfer rate (against H), (c) entropy generation, (d) Bejan number.

on entropy generation and Bejan number near to the injection wall, whereas the platelet shape has the domination tendency on entropy generation and Bejan number near to the suction wall (see Figs. 2(c), 2(d)).

Figures 3(a)–3(f) present the influence of viscous dissipation, thermal relaxation parameter, nanoparticles’ volume fraction, applied magnetic field, radiative heat flux, and frequency parameter on steady temperature of couple stress ferro nanofluid. Figure 3(a) shows that the temperature is augmenting for the magnification in viscous dissipation due to the increment in Eckert number reasons the more energy dissipation in the fluid because the enthalpy factor dwindling from the kinetic energy boosts up the thermal boundary layer thickness. Figure 3(b) depicts that the temperature is dwindling for the higher values of thermal relaxation parameter due to the increment in thermal relaxation parameter exceeding the energy transmission time between the particles which leads the fall in temperature. Figure 3(c) elucidates that the magnification in volume fraction of nanoparticles encouraging the temperature due to the higher thermal conductivity of nanoparticles. Figure 3(d) presents that the magnifying Hartmann number dwindles the temperature because the hindering forces caused by the applied magnetic field slow down the flow which leads the fall in temperature. Figure 3(e) displays that the temperature is an

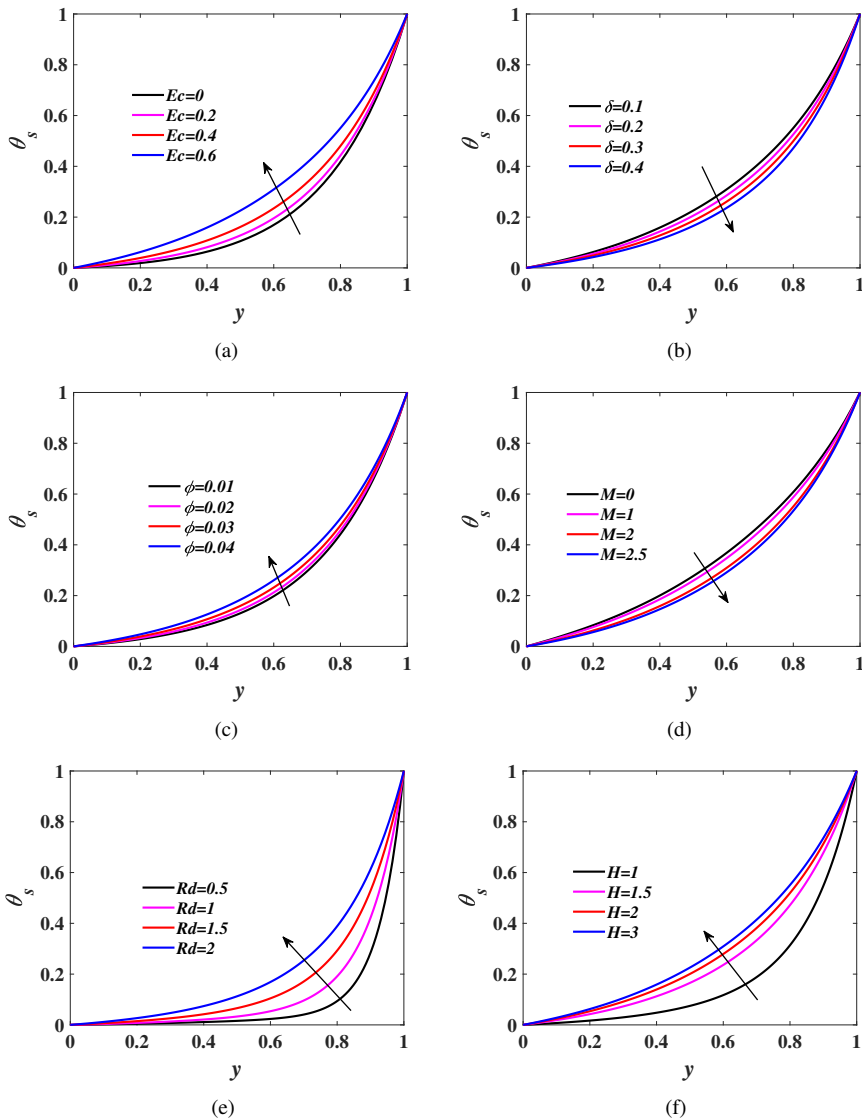


Figure 3. (a) Impression of Ec on θ_s , (b) impression of δ on θ_s , (c) impression of ϕ on θ_s , (d) impression of M on θ_s , (e) impression of Rd on θ_s , (f) impression of H on θ_s .

increasing function of thermal radiation because the increment in thermal radiation helps to improve the heat transfer from the walls to the working fluid due to the conductivity of the fluid. Figure 3(f) portrays that the acceleration in frequency parameter encourages the amplitude of the temperature.

Figures 4(a), 4(b) elevate the importance of nanoparticles' volume fraction and Hart-

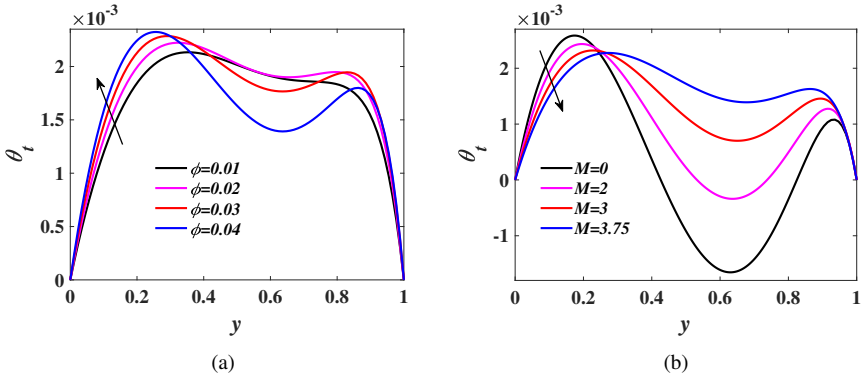


Figure 4. (a) Impact of ϕ on θ_t , (b) impact of M on θ_t .

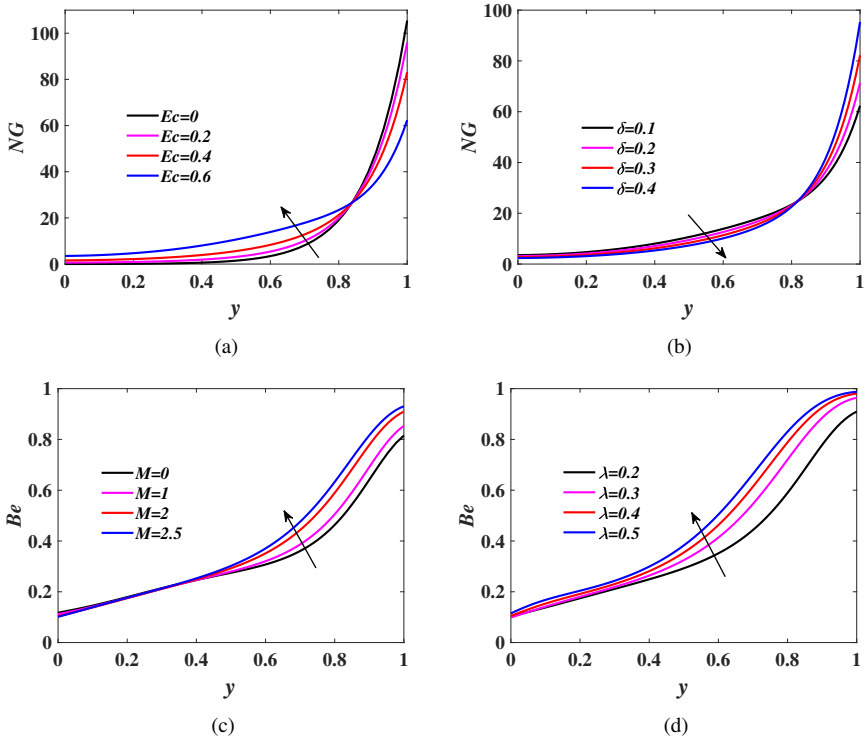


Figure 5. (a) Impression of Ec on NG , (b) impression of δ on NG , (c) impression of M on Be , (d) impression of λ on Be .

mann number on unsteady temperature. Figure 4(a) shows the magnifying nanoparticles' volume fraction rising the temperature due to the good thermal conductivity of nanoparticles. Figure 4(b) illustrates that an increment in Hartmann number dwindles

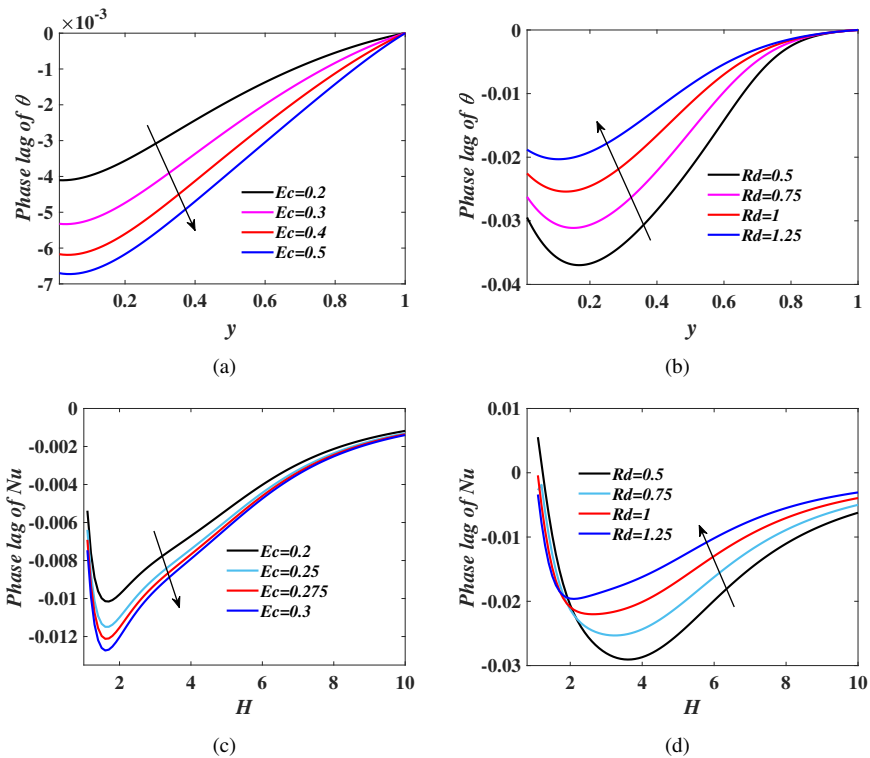


Figure 6. (a) Effect of Ec on phase lag of θ , (b) effect of Rd on phase lag of θ , (c) effect of Ec on phase lag of Nu (against H), (d) effect of Rd on phase lag of Nu (against H).

the temperature. From Figs. 4(a), 4(b) one can observe that the unsteady temperature profiles are showing oscillating nature for intensifying nanoparticles' volume fraction and Hartmann number, further, the maximum temperature is noticed in the vicinity of injection wall.

Figures 5(a), 5(b) display the influence of viscous dissipation, and thermal relaxation parameter on entropy generation. Figure 5(a) elucidates that the increment in viscous dissipation encouraging the entropy because the frictional warming from the collision of fluid molecules. Figure 5(b) shows that the rise in thermal relaxation parameter delays the energy transfer between the particles, which leads the fall in entropy. From Figures 5(a), 5(b) one can infer that the maximum entropy is noticed in the vicinity of suction wall. Figures 5(c), 5(d) portray the importance of Hartmann number, and couple stress parameter on Bejan number. The augmenting trend can be noticed in Bejan number by magnifying Hartmann number (see Fig. 5(c)), and the similar trend is true for the intensification in couple stress viscosity (see Fig. 5(d)).

The variations of phase lag of temperature and heat transfer rate (against H) are given in Figs. 6(a)–6(d) for the different values of viscous dissipation and thermal radiation. The increment in viscous dissipation boosts up the fluid inertia forces to influence for the

Table 4. Distributions of Nu_s and Nu_t at $y = 0$ for various values of λ , M , Ec , δ , Rd , and ϕ when $M = 2$, $\lambda = 0.2$, $\delta = 0.1$, $R = 1$, $H = 3$, $Pr = 21$, $Ec = 0.4$, $Rd = 2$, $Gr = 5$, $Re = 1$, $\varepsilon = 0.001$, and $t = \pi/9$.

Parameter	Values	$(Nu)_s$	$(Nu)_t$
λ	0.2	0.769085	0.000077
	0.3	0.626158	0.000053
	0.4	0.548605	0.000039
M	0	0.898780	0.000099
	1	0.861728	0.000093
	2	0.769085	0.000077
Ec	0.2	0.492996	0.000037
	0.3	0.614719	0.000057
	0.4	0.769085	0.000077
δ	0.2	0.680262	0.000064
	0.3	0.594857	0.000053
	0.4	0.513836	0.000045
Rd	1	0.047496	0.000027
	1.5	0.109578	0.000038
	2	0.238112	0.000050
ϕ	0.00	0.395090	0.000045
	0.01	0.440701	0.000051
	0.02	0.496578	0.000057

reduction in the phase of temperature (see Fig. 6(a)), whereas the reverse behaviour can be found increasing the thermal radiation (see Fig. 6(b)). Figures 6(c), 6(d) present the phase of heat transfer against H dwindles for magnifying viscous dissipation, and it rises for intensifying thermal radiation. From Figs. 6(a)–6(c) it is noticed that the maximum phase lag is found in the vicinity of suction wall. From Figs. 6(c), 6(d) one can observe that the phase lag is augmenting with amplifying frequency parameter.

The distributions of Nu_s and Nu_t at the injection wall ($y = 0$) for the influences of couple stress parameter, applied magnetic field, viscous dissipation, thermal relaxation parameter, thermal radiation, and volume fraction of nanoparticles are listed in Table 4. From this table one can infer that both the steady and unsteady Nusselt numbers are increased for magnifying viscous dissipation, thermal radiation, and the nanoparticles' volume fraction, whereas the decreasing tendency can be seen for increasing couple stress parameter, Hartmann number, and thermal relaxation parameter.

5 Conclusion

The present investigation concerned with the entropy analysis on magnetohydrodynamic couple stress ferro nanofluid flow induced by time-dependent pressure gradient between vertical porous walls with Cattaneo–Christov theory. Blood is considered as non-Newtonian fluid (couple stress fluid). The influences of Ohmic heating, viscous dissipation, and thermal radiation are considered. The present work is significant in the field of nanodrug delivery, pharmaceutical processes, dynamics of physiological fluids, microelectronics,

and biomedicines. The numerical outcomes for various parameters are presented by utilizing the shooting process with the support of the 4th-order Runge–Kutta procedure. The major results of the current investigation are shortened here:

- Spherical shape nanoparticles have high heat transfer rate compare to other shapes.
- The increment in thermal relaxation parameter declines the temperature, whereas the reverse behavior can be found with intensifying viscous dissipation, thermal radiation, and frequency parameter.
- Heat transfer rate increases with the boost up in viscous dissipation, and thermal radiation, while it decreases with the increment in couple stress parameter and Hartmann number.
- Entropy escalates for intensifying viscous dissipation, whereas the opposite trend can be found for the high values of thermal relaxation parameter.
- Bejan number is enhancing with the escalation in Hartmann number and couple stress parameter.
- Phase lag of heat transfer rate reduces with magnifying viscous dissipation, and it enhances with intensifying thermal radiation.

References

1. S.O. Adesanya, O.D. Makinde, Effects of couple stresses on entropy generation rate in a porous channel with convective heating, *Comput. Appl. Math.*, **34**(1):293–307, 2015, <https://doi.org/10.1007/s40314-014-0117-z>.
2. H.T. Basha, R. Sivaraj, Exploring the heat transfer and entropy generation of Ag/Fe₃O₄-blood nanofluid flow in a porous tube: A collocation solution, *Eur. Phys. J. E*, **44**(3):1–24, 2021, <https://doi.org/10.1140/epje/s10189-021-00024-x>.
3. C. Cattaneo, Sulla conduzione del calore, *Atti Sem. Mat. Fis. Univ. Modena.*, **3**:83–101, 1948, <https://cir.nii.ac.jp/crid/1573950400546202112>.
4. P. Chaturani, R.P. Samy, Pulsatile flow of Casson’s fluid through stenosed arteries with applications to blood flow, *Biorheology*, **23**(5):499–511, 1986, <https://doi.org/10.3233/BIR-1986-23506>.
5. S.U.S. Choi, Nanofluids: From vision to reality through research, *J. Heat Transfer*, **131**:033106, 2016, <https://doi.org/10.1115/1.3056479>.
6. C.I. Christov, On frame indifferent formulation of the Maxwell-Cattaneo model of finite-speed heat conduction, *Mech. Res. Commun.*, **36**:481–486, 2009, <https://doi.org/10.1016/j.mechrescom.2008.11.003>.
7. M. Devakar, T.K.V. Iyengar, Stokes’ problems for an incompressible couple stress fluid, *Nonlinear Anal. Model. Control*, **13**(2):181–190, 2008, <https://doi.org/10.15388/NA.2008.13.2.14578>.
8. M.H. Esfe, M. Bahiraei, A. Torabi, M. Valadkhani, A critical review on pulsating flow in conventional fluids and nanofluids: Thermo-hydraulic characteristics, *Int. Commun. Heat Mass Transf.*, **120**:104859, 2021, <https://doi.org/10.1016/j.icheatmasstransfer.2020.104859>.

9. J.B. Fourier, La théorie analytique de la chaleur, *Mem. Acad. R. Sci.*, **8**:581–622, 1829, https://www.academie-sciences.fr/pdf/dossiers/Fourier/Fourier_publici.htm.
10. N.S. Gad, Effect of Hall currents on interaction of pulsatile and peristaltic transport induced flows of a particle–fluid suspension, *Appl. Math. Comput.*, **217**(9):4313–4320, 2011, <https://doi.org/10.1016/j.amc.2010.08.016>.
11. K. Govindarajulu, A.S. Reddy, Magneto hydrodynamic pulsatile flow of third grade hybrid nanofluid in a porous channel with Ohmic heating and thermal radiation effects, *Phys. Fluids*, **34**:013105, 2022, <https://doi.org/10.1063/5.0074894>.
12. M. Habibishandiz, M.Z. Saghir, A critical review of heat transfer enhancement methods in the presence of porous media, nanofluids, and microorganisms, *Therm. Sci. Eng. Prog.*, **30**:101267, 2022, <https://doi.org/10.1016/j.tsep.2022.101267>.
13. D. Hacen, K. Slimi, S.B. Nasrallah, Entropy generation for pulsating flow in a composite fluid/porous system, *J. Porous Media*, **11**(6), 2008, <https://doi.org/10.1615/JPorMedia.v11.i6.40>.
14. R.L. Hamilton, O.K. Crosser, Thermal conductivity of heterogeneous two-component systems, *IEC Fundamentals*, **1**(3):187–191, 1959, <https://doi.org/10.1021/i160003a005>.
15. K.H. Hosseinzadeh, S.O. Roghani, A. Asadi, A. Mogharrebi, D.D. Ganji, Investigation of micropolar hybrid ferrofluid flow over a vertical plate by considering various base fluid and nanoparticle shape factor, *Int. J. Numer. Methods Heat Fluid Flow*, **31**:402–417, 2021, <https://doi.org/10.1108/HFF-02-2020-0095>.
16. C.K. Kumar, S. Srinivas, A.S. Reddy, MHD pulsating flow of Casson nanofluid in a vertical porous space with thermal radiation and Joule heating, *J. Mech.*, **36**:535–549, 2020, <https://doi.org/10.1017/jmech.2020.5>.
17. C. Kumawat, B.K. Sharma, Q.M. Al-Mdallal, M. Rahimi-Gorji, Entropy generation for MHD two phase blood flow through a curved permeable artery having variable viscosity with heat and mass transfer, *Int. Commun. Heat Mass Transf.*, **133**:105954, 2022, <https://doi.org/10.1007/s10237-022-01561-w>.
18. G. Radhakrishnamacharya, M.K. Maiti, Heat transfer to pulsatile flow in a porous channel, *Int. J. Heat Mass Transf.*, **20**(2):171–173, 1977, [https://doi.org/10.1016/0017-9310\(77\)90009-6](https://doi.org/10.1016/0017-9310(77)90009-6).
19. S. Rajamani, A.S. Reddy, Effects of Joule heating, thermal radiation on MHD pulsating flow of a couple stress hybrid nanofluid in a permeable channel, *Nonlinear Anal. Model. Control*, **27**(4):684–699, 2022, <https://doi.org/10.15388/namc.2022.27.26741>.
20. Z. Said, L.S. Sundar, A.K. Tiwari, H.M. Ali, M. Sheikholeslami, E. Bellos, H. Babar, Recent advances on the fundamental physical phenomena behind stability, dynamic motion, thermophysical properties, heat transport, applications, and challenges of nanofluids, *Phys. Rep.*, **946**:1–94, 2022, <https://doi.org/10.1016/j.physrep.2021.07.002>.
21. B.K. Sharma, R. Gandhi, M.M. Bhatti, Entropy analysis of thermally radiating MHD slip flow of hybrid nanoparticles (Au-Al₂O₃/blood) through a tapered multi-stenosed artery, *Chem. Phys. Lett.*, **790**:139348, 2022, <https://doi.org/10.1016/j.cplett.2022.139348>.

22. H.M. Shawky, Pulsatile flow with heat transfer of dusty magnetohydrodynamic Ree-Eyring fluid through a channel, *Heat Mass Transf.*, **45**(10):1261–1269, 2009, <https://doi.org/10.1007/s00231-009-0502-0>.
23. M. Sheikholeslami, Z. Shah, A. Tassaddiq, A. Shafee, I. Khan, Application of electric field for augmentation of ferrofluid heat transfer in an enclosure including double moving walls, *IEEE Access*, **7**:21048–21056, 2019, <https://doi.org/10.1109/ACCESS.2019.2896206>.
24. S. Srinivas, C.K. Kumar, A.S. Reddy, Dufour and Soret effects on pulsatile hydromagnetic flow of Casson fluid in a vertical non-Darcian porous space, *Nonlinear Anal. Model. Control*, **27**(4):669–683, 2022, <https://doi.org/10.15388/namc.2022.27.26678>.
25. D. Srinivasacharya, G.M. Rao, Pulsatile flow of couple stress fluid through a bifurcated artery, *Ain Shams Eng. J.*, **9**(4):883–893, 2018, <https://doi.org/10.1016/j.asej.2016.04.023>.
26. V.K. Stokes, Effects of couple stresses in fluids on hydromagnetic channel flows, *Phys. Fluids*, **11**(5):1131–1132, 1968, <https://doi.org/10.1063/1.1692056>.
27. E.V. Timofeeva, J.L. Routbort, D. Singh, Particle shape effects on thermophysical properties of alumina nanofluids, *J. Appl. Phys.*, **106**(1):014304, 2009, <https://doi.org/10.1063/1.3155999>.
28. C.Y. Wang, Pulsatile flow in a porous channel, *J. App. Mech. Trans. ASME.*, **38**(2):553–555, 1971, <https://doi.org/10.1115/1.3408822>.
29. X. Wang, Y. Qiao, H. Qi, H. Xu, Numerical study of pulsatile non-Newtonian blood flow and heat transfer in small vessels under a magnetic field, *Int. Commun. Heat Mass Transf.*, **133**:105930, 2022, <https://doi.org/10.1016/j.icheatmasstransfer.2022.105930>.
30. H. Waqas, T. Muhammad, S. Noreen, U. Farooq, M. Alghamdi, Cattaneo-Christov heat flux and entropy generation on hybrid nanofluid flow in a nozzle of rocket engine with melting heat transfer, *Case Stud. Therm. Eng.*, **28**:101504, 2021, <https://doi.org/10.1016/j.csite.2021.101504>.
31. Q. Ye, Y. Zhang, J. Wei, A comprehensive review of pulsating flow on heat transfer enhancement, *Appl. Therm. Eng.*, **196**:117275, 2021, <https://doi.org/10.1016/j.applthermaleng.2021.117275>.